Electronic Structure, Electronic Charge Density and Optical Properties of Organic –Inorganic Hybrid Semiconductor C$_2$H$_6$NTeZn

Wilayat Khan[1], Sikander Azam[1], Saleem Ayaz Khan[1], A. H. Reshak[1,2]

[1] New Technologies-Research Center, University of West Bohemia, Univerzitni 8, 306 14 Pilsen, Czech Republic

[2] Center of Excellence Geopolymer and Green Technology, School of Material Engineering, University Malaysia Perlis, 01007 Kangar, Perlis, Malaysia

[*]Corresponding author: *Wilayat Khan,*

Abstract: The electronic structure, electronic charge density and optical properties of the organic –inorganic hybrid semiconductor C$_2$H$_6$NTeZn are premeditated by employing the full-potential density-functional technique. The band structure of our optimize crystal indicate semiconductor nature. For understanding the nature of chemical bonding in the investigated material, we calculate the electronic charge density in (110) and (010) crystallographic planes. From the density of states (DOS) study we emphasize that in the PDOS, the valence band maximum (VBM) is contributed strongly from the Zn-d state and a minor contribution from the hybridization of N-s and C-s states. The conduction band minimum is mainly formed from the Zn-s orbital while on the other hand small contribution from Te-p and Te-s states. Further more, we also have calculated the optical properties, to get a physical basis for latent application in optoelectronic devices.

Keyword: Band structure; Density of states; electronic charge density; Optical properties: DFT

I. INTRODUCTION

Crystalline mixtures constructed up of periodically ordered nanostructured inorganic semiconductor motifs and organic molecules are an innovative kind of hybrid semi conducting components that are of large basic significance and technological relevance [1-9]. The mainly interesting characteristic of these components is that many complimentary properties of each individual constituent are conveyed into the hybrid structure by embedding two noticeably different constituents into a single crystal lattice. Integration and blending of outstanding transport properties and structural/thermal firmness from the inorganic constituent and excellent flexibility and possibility from the organic constituent can be anticipated. Moreover, the combining of the inorganic and organic modules in these crystalline hybrid molecules takes location at the atomic level and through chemical bonds, and therefore is free of the interface issues that are unavoidably present in accepted hybrid composite components. In addition, the configuration of such hybrid crystals nearly always leads to exclusive and remarkable new characteristics that are not possible for the one-by-one constituents. Some prominent demonstrations include organic–inorganic perovskite-like structures and associated materials [1-4] hybrid metal oxides [5, 6] and semiconductors created of zinc blende and wurtzite frameworks [7-9]. The II/VI based hybrid semiconductor crystal structures (II: Group 12 components and Mn; VI: Group 16 components) are composed of one-dimensional (1D) chains or two-dimensional (2D) slabs of II/VI semiconductor fragments that are interconnected or divided by organic amine substances to form periodic crystal lattices. They are of the common equation [MQ(L)$_x$] (M=Mn, Zn, Cd; Q=S, Se, Te; L=organic amine or diamine; and x=0.5, 1). The most captivating explanation encompass exceedingly powerful band-edge absorption (e.g. 10–20 times higher than bulk II/VI and GaAs) and remarkably large band-gap tunability (0.1–2.0 eV) as a consequence of very powerful

structure-induced quantum confinement [10, 12] even though, according to theoretical computation [10], the organic spacers grant rise to a very restricted effect on the band-gap-related electrical devices and optical properties, they play a vital function in the structural, mechanical, and thermal behaviors of these hybrid components. In 2009 Xiaoying Huang et. al. [11] reported five crystal structures of 3D-[ZnTe(L)$_{0.5}$] prepared of ZnTe single-atomic slabs and long chain diamines, in addition to their functional stage transitions, mechanical properties, accurate heat capability, thermal diffusivity, and thermal conductivity. Our analysis displays that crystalline hybrid semiconductors of this kind are much lighter and considerably more bendable than their inorganic corresponding items. The amalgamation of organic substances into the semiconductor crystal lattices also leads to drastically decreased thermal conductivity that is most attractive for high concert thermoelectric materials with functional integrity [12-16].

In this article, we analyze the electronic structure, electronic charge density and optical properties of C_2H_6NTeZn compound within the modified Becke and Johnson (mBJ) [17] exchange correlation energy within the framework of full-potential linearized augmented plane wave (FP-LAWP) technique as employed in the WIEN2K package [18].

II. CRYSTAL STRUCTURE AND COMPUTATIONAL DETAIL

For our calculations we use the lattice parameters of the organic –inorganic hybrid semiconductor a-ZnTe(bda)$_{0.5}$, given in the crystallographic data (CCDC-736292) [19]. Our investigated compound has monoclinic symmetry with space group $P2_1/c$, having eight formulas/unit cell. The molecular structure of the investigated compound is shown in Fig. 1.

The full-potential linearized augmented plane wave (FP-LAPW) technique is used to calculate the electronic structure and linear optical properties of C_2H_6NTeZn compound, which is based on density functional theory (DFT) as employed in the WIEN2K package [20]. We carried out the DFT calculations for optimizing the structure of our investigated compound by minimizing the forces acting on each atom of C_2H_6NTeZn compound to get stable geometry. The structure of the crystal is considered to be stable when the convergence of energy criterion 1mRy/a.u. The self consistency is achieved at 10^{-4}Ry. For our calculations, we choose the R$_{MT}$ values in such a way that no charge leakage is observed from the core and also the convergence of the total energy was ensured. The Muffin Tin (MT) sphere is expanded up to *lmax*=10, inside which the potential and charge density is indicated. We set the value R$_{MT}$K$_{MAX}$=7, for the expansion of the basis function.

The electronic exchange-correlation energy is solved by using local density approximation (LDA) [21], generalized gradient approximation (GGA) [22] and Engle Vosko generalized gradient approximation (EV-GGA) [23]. In order to avoid the underestimation of LDA and GGA, we have used the modified Becke-Johnson approximation (mBJ) to get better band gap value. The below equation give mBJ potential and its explanation is found in the Refs [24, 17, 25].

$$v_{X,\sigma}^{MBJ}(r) = cv_{X,\sigma}^{BR}(r) + (3c-2)\frac{1}{\pi}\sqrt{\frac{5}{12}}\sqrt{\frac{2t_\sigma(r)}{\rho_\sigma(r)}} \qquad (1)$$

Where $\rho_\sigma = \sum_{i=1}^{N_\sigma}\left|\psi_{i,\sigma}\right|^2$ represent the electron density, $t_\sigma = (1/2)\sum_{i=1}^{N_\sigma}\nabla\psi_{i,\sigma}^*.\nabla\psi_{i,\sigma}$ stands for kinetic energy density and $v_{X,\sigma}^{MBJ}$ stand for the Becke-Roussel (BR) potential [27].
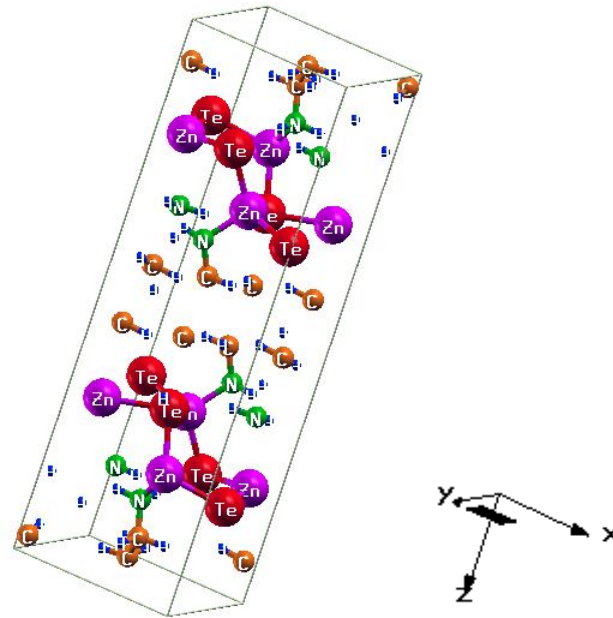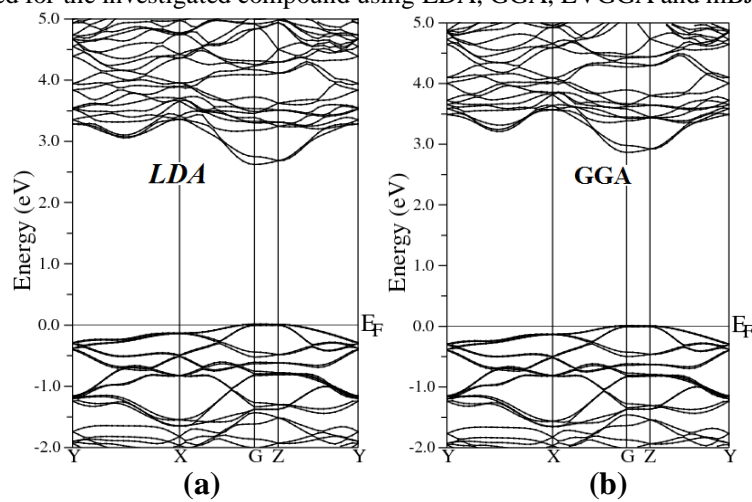
Fig. 1: Molecular structures of C_2H_6NTeZn compound

III. RESULTS AND DISCUSSION

Electronic structure

To examine the electronic and optical properties of a compound, it is very useful to investigate the band structure. The band structure has been calculated for the investigated compound using LDA, GGA, EVGGA and mBJ (see Fig. 2).
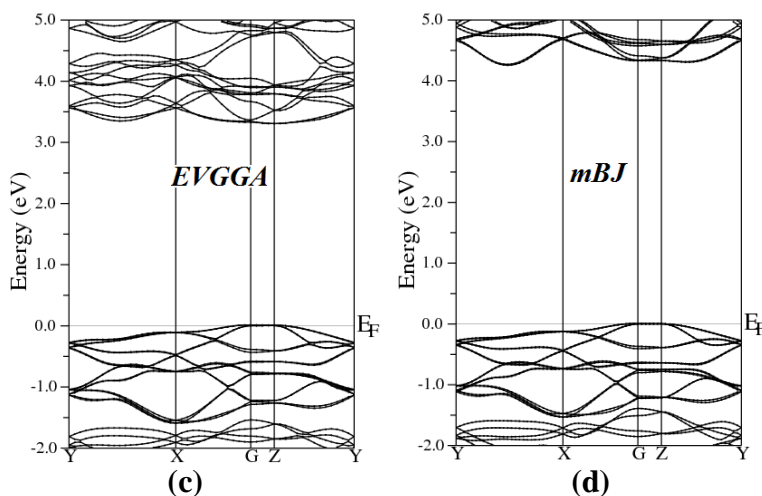
(c)   **(d)**

Fig. 2 Calculated band structures of C_2H_6NTeZn compound using LDA, GGA, EVGGA and mBJ

Figure 2 (a, b, c and d) shows the band structure of the investigated compound along the selected high-symmetry lines within the first Brillouin zone of the monoclinic crystal. The symbols is assign to high symmetry points of irreducible Brillioun zone (IBZ). Following Fig. 2, it is clear that our investigated compound is a direct band gap semiconductor. From these results we conclude that mBJ give better band gap [27-31] value as compared to other approximation i.e. LDA, GGA and EVGGA. Due to this reason, mBJ is taken as a best tool for calculating the band gap. The calculated energy band gap for the four approximations (LDA, GGA, EVGGA and mBJ) is displayed in the Table 1.

Table.1 calculated band gaps of C_2H_6NTeZn, using LDA, GGA, EVGGA and mBJ

C_2H_6NTeZn	LDA	GGA	EVGGA	mBJ
E_g (eV)	2.79	2.93	3.322	4.25

From the total density of states (TDOS) and partial density of states (PDOS), we can visualize the atomic states hybridization and contributions to the band in the band structure of C_2H_6NTeZn compound. Fig. 3(a, b, c, d, e and f) report the calculated TDOS by using LDA, GGA, EVGGA and mBJ approximations. Since we state that the mBJ give better band splitting thus for the calculation of PDOS we have demonstrated the results obtained by mBJ (Fig. 3). We should emphasize that in the PDOS, the valence band maximum (VBM) is contributed strongly from the Zn-d states with a minor contribution of N-s and C-s states and possess a strong hybridization between N-s and C-s states. Fig. 3 shows that the energy range from -5.0 eV to 0.0 eV is mainly due to the contribution of Te-p, Zn-s and N-p states with small contribution of the remaining states. The lowest part of the valence band from -10.0 eV to -5.0 eV is due to the Te-s and Zn-d states provide the greater contribution as compared to other states i.e N-s, C-s, Zn-s, Zn-p, H-s and Te-p, Te-d which shows negligible contribution (Fig. 3). The conduction band minimum is mainly from the Zn-s orbital with the small contribution of Te-p and Te-s states.
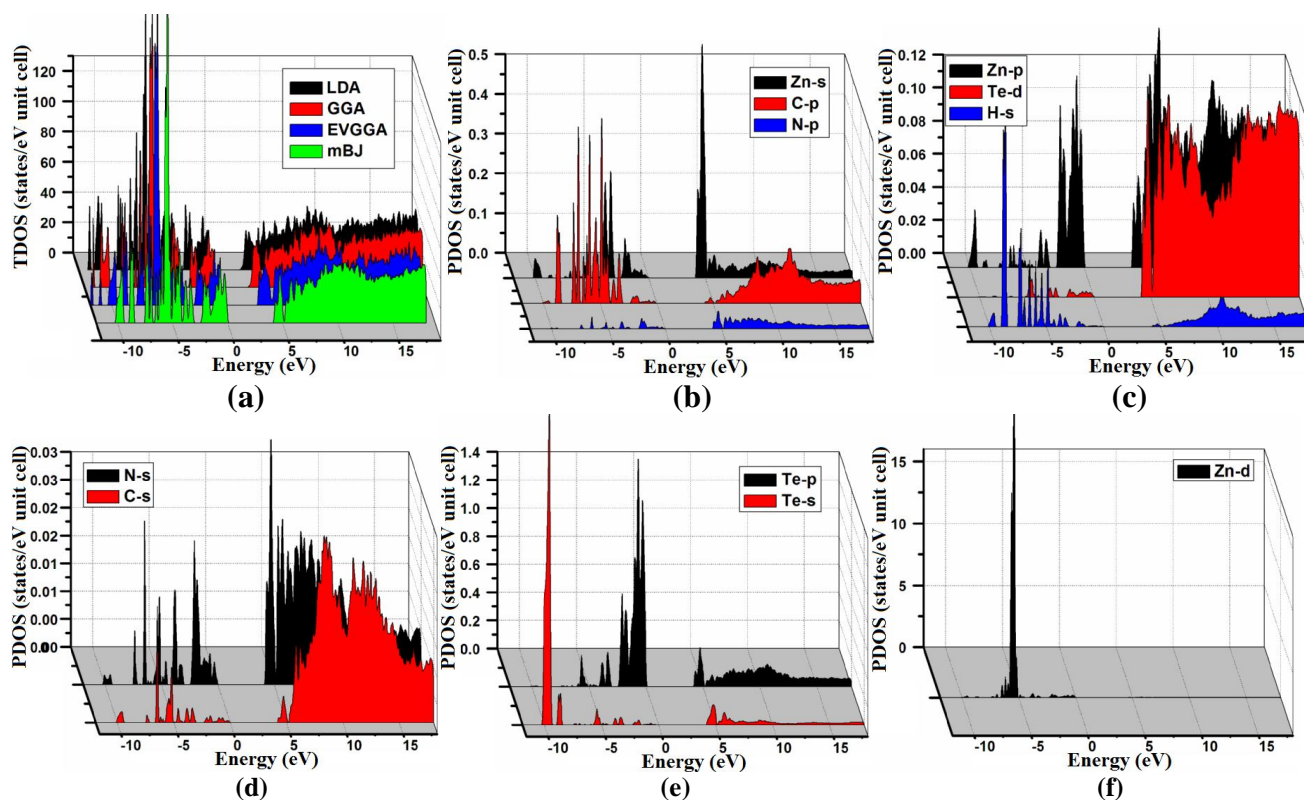
Fig. 3 Calculated total density state (DOS) and partial density of states (PDOS) of C_2H_6NTeZn compound using mBJ

Electronic charge density

In order to understand the chemical bonding nature of the organic –inorganic hybrid semiconductor C_2H_6NTeZn, we calculate the electronic charge density using mBJ approximation in (110) and (010) crystallographic planes (Fig. 4(a, b). It is clear from the Fig. 4 that Te atom shows ionic nature of chemical bonding, which surround by spherical lines. The values of electro negativity of Carbon, Hydrogen, Nitrogen, Tellurium, and Zinc are 2.55, 2.20, 3.04, 2.1 and 1.65, respectively. The electro negativity difference between two atoms is used to find the bonding nature. The electro negativity difference between Te and Zn is 0.94 indicate polar covalent bond. On the other hand the difference in the electronegativity of C and H atoms is 0.30 shows the strong sharing of electrons and the same bond is also appeared between N and H atoms. It is also clear from the Fig. 4 that there is polar covalent bond between Zn and C atoms. According to thermo scale the blue color represents greater concentration of charge (+1.0000), that's why the carbon atom displays maximum charge concentration as compared to other atoms. The crystallographic planes (110) and (010) show considerable anisotropy (see Fig. 4).
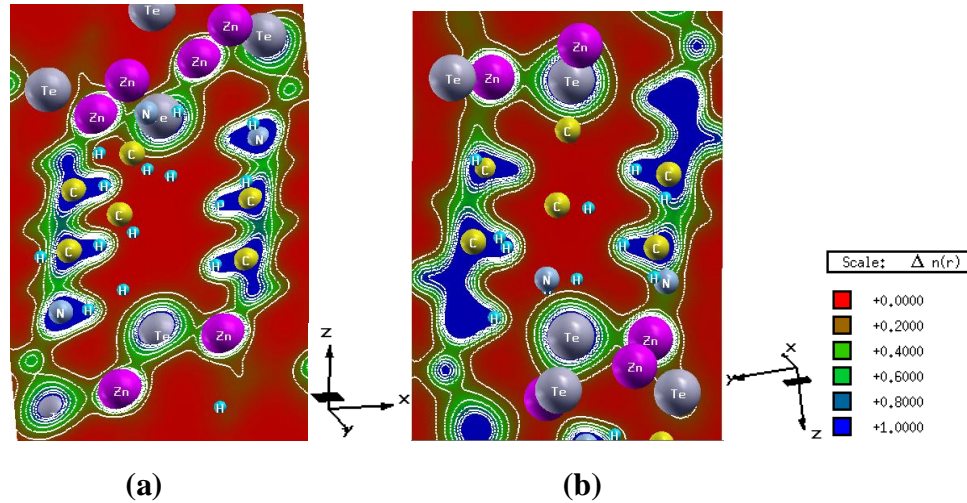
(a)　　　　　　　　**(b)**

Fig. 4 Electronic charge density distribution contour calculated with mBJ in the (010) and (010) planes of of C_2H_6NTeZn compound using mBJ

Optical Properties

The complex dielectric function explains the linear behavior of the system to an electromagnetic radiation. All optical spectra of C_2H_6NTeZn organic –inorganic hybrid semiconductor, including real $\varepsilon_1(\omega)$ and imaginary $\varepsilon_2(\omega)$ parts of dielectric tensor, reflectivity $R(\omega)$, refractive index $n(\omega)$, extension coefficient $K(\omega)$, optical conductivity $\sigma(\omega)$, energy loss function $L(\omega)$ and absorption co-efficient $I(\omega)$ are calculated and analyzed in detail. The dielectric tensor components for C_2H_6NTeZn compound is calculated for both parallel and perpendicular direction of electromagnetic radiation polarization. The momentum matrix elements calculate electron transitions between the occupied and unoccupied states following the selection rules [32], that result the imaginary part $\varepsilon_1(\omega)$ of dielectric function which is given by ;

$$\operatorname{Im}\varepsilon_{\alpha\beta}^{\{inter\}}(\omega) = \frac{\hbar^2 e^2}{\pi m^2 \omega^2} \sum_n \int dk \left\langle \psi_k^{c_n} \left| p^\alpha \right| \psi_k^{v_n} \right\rangle \left\langle \psi_k^{c_n} \left| p^\beta \right| \psi_k^{v_n} \right\rangle \delta\left(E_K^{c_n} - E_K^{c_n} - \omega\right) \qquad (2)$$

where p represents the momentum matrix element of the crystals with momentum k.

The symbols $E_k^{c_n}$ and $E_k^{v_n}$ represent the energy for the conduction and valence bands, respectively. The absorption spectrum is proportional to the total inter-band transitions from the filled valence states $\psi_k^{c_n}$ to vacant conduction states $\psi_k^{v_n}$ over the K-points of the 1st Brillouin zone. The real part of the dielectric function $\varepsilon_1(\omega)$ is obtained from the imaginary part of the dielectric function $\varepsilon_2(\omega)$ by using the Kramers–Kronig transformation:

$$\operatorname{Re}\varepsilon_{\alpha\beta}^{\{inter\}}(\omega) = \delta_{\alpha\beta} + \frac{2}{\pi} p \int_0^\infty \frac{\omega \operatorname{Im}\varepsilon_{\alpha\beta}(\omega)}{\omega'^2 - \omega^2} d\omega \qquad (3)$$

The inter-band transition is taken into account during the calculation of the real and imaginary part of the dielectric function of C_2H_6NTeZn compound for parallel and perpendicular direction of electric field, as shown in Fig. 5, using mBJ. Our investigated crystal C_2H_6NTeZn posses monoclinic symmetry, therefore it contains three nonzero principal dielectric tensor components of second order, as follow $\varepsilon^{xx}(\omega)$, $\varepsilon^{yy}(\omega)$ and $\varepsilon^{zz}(\omega)$. Fig. 5a, shows the plots of $\varepsilon_2^{xx}(\omega)$, $\varepsilon_2^{yy}(\omega)$ and $\varepsilon_2^{zz}(\omega)$, which is obtained by using mBJ approach. The imaginary part $\varepsilon_2(\omega)$ of dielectric function indicates several peaks in the small energy ranging from 4.6 to 7.0 eV and the main peaks appeared at 5.37 eV for $\varepsilon_2^{xx}(\omega)$, 5.14 eV for $\varepsilon_2^{yy}(\omega)$ and 6.4 for $\varepsilon_2^{zz}(\omega)$ originated due to the transitions from Te-p states to Zn-s states. A considerable anisotropic behavior is found among the three spectral components of dielectric tensor (Fig. 5a).

The real part of the dielectric tensor components $\varepsilon_1^{xx}(\omega)$, $\varepsilon_1^{yy}(\omega)$, and $\varepsilon_1^{zz}(\omega)$, as shown in the Fig. 5b. The calculated static values of the three components $\varepsilon_1^{xx}(0)$, $\varepsilon_1^{xx}(0)$ and $\varepsilon_1^{xx}(0)$ are 3.07, 3.24 and 2.91, respectively. Our investigated compound possess a band gap of about 4.26 eV, resulting smaller value of $\varepsilon_1(0)$,which is explained on the basis of Penn model [33]. The Penn model is given by the following relation;

$$\varepsilon(0) \approx 1 + \left(\hbar\omega / E_g\right)^2 \qquad\qquad (4)$$

It is clear from equation (3) that $\varepsilon(0)$ is inversely proportional to E_g. The compound which has smaller value of band gape exhibit larger value of $\varepsilon(0)$.
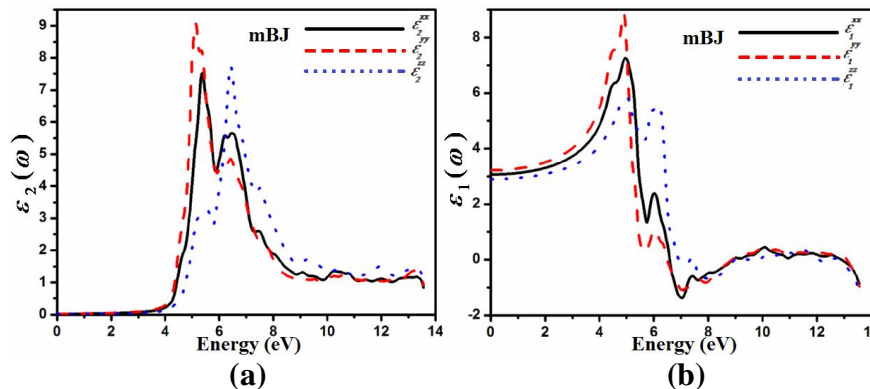

Fig. 5 Calculated real and imaginary parts of dielectric functions, using mBJ

By knowing the real and imaginary part of dielectric function we can calculate the remaining optical properties like, the reflectivity R(ω), optical conductivity $\sigma(\omega)$, refractive index n(ω), extension co-efficient k(ω), absorption co-efficient I(ω) and energy loss function L(ω),respectively.

Fig. 5(c), represent the reflectivity spectra $R^{xx}(\omega)$, $R^{yy}(\omega)$ and $R^{zz}(\omega)$ as a function of energy. The static values of reflectivity are 4.5 %, 5.0 % and 2.0 % for $R^{xx}(\omega)$, $R^{yy}(\omega)$ and $R^{zz}(\omega)$, respectively. for higher energy (13.5 eV) the three components show maximum reflectivity of 50 %.

The variation in the real Reσ and imaginary Imσ part of the optical conduction as a function of photon energy $\hbar\omega$, as shown in Fig. 5(d, e). The optical conductivity $\sigma(\omega)$ plots indicate big variation at small energy spectrum. The real part of conductivity $\sigma^{xx}(\omega)$, $\sigma^{yy}(\omega)$ and $\sigma^{zz}(\omega)$ show maximum value around 5.0 eV and 6.0 eV. Two valleys are appeared which are corresponding to the peaks of imaginary part of the conductivity at about the same energies (Fig. 5(d, e). It is clear from the Fig. 5(d, e), that the same behavior is observed in both part of conductivity at higher energy along the spectral region.

Fig. 5f, shows the refractive index n(ω) as a function of energy. The static values of refractive index $n^{xx}(0)$, $n^{xx}(0)$ and $n^{xx}(0)$ are found to be 1.73, 1.78, and 1.69, respectively. It is clear from Fig. 5f, the amplitude increases with energy in the absorption region, and reach its maximum in far ultraviolet region (at about 5.0 eV). At higher energy, beyond 6.0 eV, it tends to decrease and achieve its minimum value at 8.0 eV. One can see from Fig. 5f, that there is a considerable anisotropy among the three components ($n^{xx}(\omega)$,$n^{xx}(\omega)$ and $n^{xx}(\omega)$) of the refractive index.

The extinction coefficient k(ω) is displayed in Fig. 5g. k(ω), possess maximum peaks in the energy range between 4.8 eV and 7.0 eV. The energy loss function L(ω) is plotted in Fig. 5h, which exhibit peaks located at energy around 12.6 eV corresponding to the abrupt decrease in the spectrum of reflectivity R(ω). The maximum peaks in L(ω) is corresponding to the screened plasma ω_p [34]. The z-component of the energy loss function show considerable anisotropy with the other two components along the spectral region (Fig. 5h). Fig. 5i, reports the absorption co-efficient I(ω). It is obvious from Fig. 5i, that the spectral components of absorption co-efficient $I^{xx}(\omega)$ and $I^{yy}(\omega)$ show isotropic behavior and the $I^{zz}(\omega)$ shows considerable anisotropy with $I^{xx}(\omega)$ and $I^{yy}(\omega)$ in the energy range from 5.0 eV to 13.0 eV. One can note that the $I^{xx}(\omega)$

exhibit maximum value at 7.0 eV and beyond 13.0 eV i.e. at higher energy $I^{zz}(\omega)$ indicate higher value as compared to other two components.
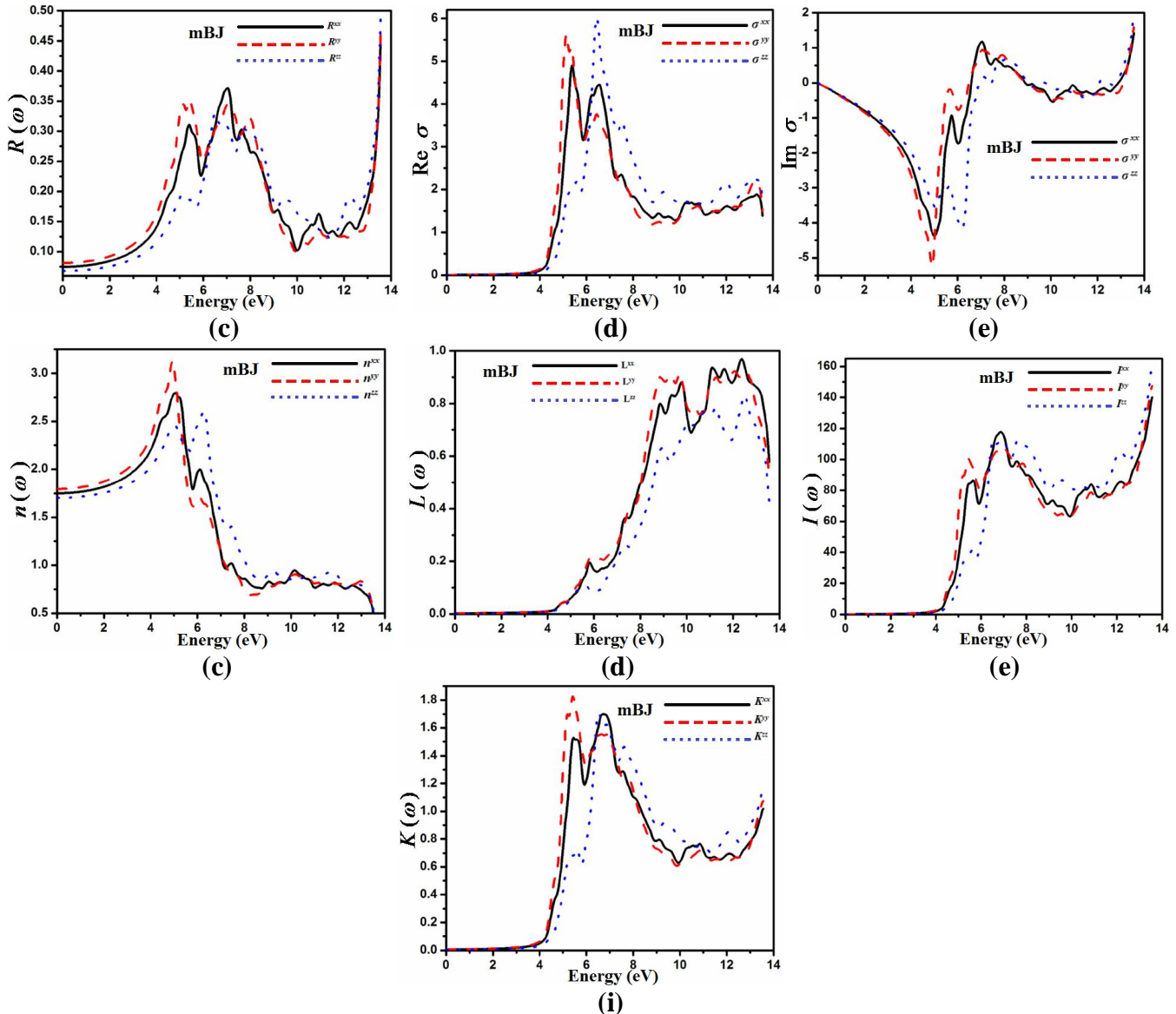

Fig. 5 Reflectivity, refractive index, extension co-efficient, absorption coefficient, optical conductivity and energy loss function of C_2H_6NTeZn compound using mBJ

IV. CONCLUSION

We studied the electronic structure, electronic charge density and linear optical properties of the organic–inorganic hybrid semiconductor C_2H_6NTeZn, using the first principle calculation. Our calculated results for the band structure indicate direct

band gap of about 4.25 eV, using mBJ, which provide better band splitting than the other three approximations. The Te-p, Zn-s and N-p states posses' main contribution to the upper part of the valence band, while the lower part of the conduction band is highly contributed by Zn-s orbital with the small support of Te-p and Te-s states. Our calculated electronic charge density repots strong sharing of electrons between C/N with H atoms. We examine that our calculated optical properties show anisotropic nature at the middle of the spectral region. The calculated results of the optical properties show that the C_2H_6NTeZn is suitable for optoelectronic devices.

Acknowledgements

REFERENCES

[1] Kagan, C. R., Mitzi, D. B., and Dimitrakopoulos, C. D., "Organic-Inorganic Hybrid Materials as Semiconducting Channels in Thin-Film Field-Effect Transistors", Science, vol. 286, pp. 945-947, 1999.

[2] Mitzi, D. B., "In Progress in Inorganic Chemistry", Vol. 48 (Ed.: K. D. Karlin), Wiley, New York, p. 1, 1999.

[3] Mitzi, D. B., and Kagan, C. R., "In Thin-Film Transistors", (Eds.: C. R. Kagan, P. Andry), Marcel Dekker, New York, pp. 475 2003.

[4] Ishihara, T., "In Optical properties of Low-Dimensional Materials", Vol. 1 (Eds.: T. Ogawa, Y. Kanemitsu), World Scientific, Singapore. pp. 289 – 335 1996.

[5] Johnson, J. W., Jacobson, A. J., Rich, S. M., and Brody, J. F., "New layered compounds with transition-metal oxide layers separated by covalently bound organic ligands. Molybdenum and tungsten trioxide-pyridine", J. Am. Chem. Soc, vol. 103, pp. 5246-5247, 1981.

[6] Yan, B. B., Xu, Y., Goh, N. K., and Chia, L. S., "Hydrothermal synthesis and crystal structures of two novel hybrid open-frameworks and a two-dimensional network based on tungsten(VI) oxides", Chem. Commun, pp.2169-2170, 2000.

[7] Huang, X. Y., Li, J., and Fu, H., "The First Covalent Organic−Inorganic Networks of Hybrid Chalcogenides: Structures That May Lead to a New Type of Quantum Wells", J. Am. Chem. Soc, vol. 122, pp. 8789-8790, 2000.

[8] Huang, X. Y., Heulings, H. R., Le, V., and Li, J., "Inorganic−Organic Hybrid Composites Containing MQ (II−VI) Slabs: A New Class of Nanostructures with Strong Quantum Confinement and Periodic Arrangement", Chem. Mater, vol. 13, pp. 3754-3759, 2001.

[9] Huang, X. Y., Li, J., Zhang, Y., and Mascarenhas, A., "From 1D Chain to 3D Network: Tuning Hybrid II-VI Nanostructures and Their Optical Properties", J. Am. Chem. Soc, vol. 125, pp. 7049-7055, 2003.

[10] Fu, H., and Li, J., "Density-functional study of organic–inorganic hybrid single crystal ZnSe$(C2H8N2)1/2$", J. Chem. Phys, vol. 120, pp. 6721 2004.

[11] Li, J., et al., "Flexible Hybrid Semiconductors with Low Thermal Conductivity: The Role of Organic Diamines", Angew. Chem. Int. Ed. vol. 48, pp. 7871 –7874 2009.

[12] Fluegel, B., Zhang, Y., Mascarenhas, A., Huang, X. Y., and Li, J., "Electronic properties of hybrid organic–inorganic semiconductors", Phys. Rev. B, vol.70, pp. 205308-12, 2004.

[13] Zhang, Y., Dalpian, G. M., Fluegel, B., Wei, S. H., Mascarenhas, A., Huang, X. Y., Li, J., and Wang, L. W., "Novel Approach to Tuning the Physical Properties of Organic-Inorganic Hybrid Semiconductors", Phys. Rev. Lett, vol. 96, pp. 026405-026409, 2006.

[14] Dresselhaus, M. S., Chen, G., Tang, M. Y., Yang, R. G., Lee, H., Wang, D. Z., Ren, Z. F., Fleurial, J. P., and Gogna, P., "New Directions for Low-Dimensional Thermoelectric Materials", Adv. Mate, vol. 19, pp. 1043-1053 (2007).

[15] Goldsmid, H. J., "Thermoelectric Refrigeration", Plenum, New York, 1964.

[16] Rowe, D. M., "Thermoelectrics Handbook: Macro to Nano", CRC, Boca Raton 2005.

[17] Becke A. D., and Johnson, E. R., "A simple effective potential for exchange", J. Chem. Phys, vol. 124, pp. 221101, 2006.

[18] Becke A. D., and Roussel, M. R., "Exchange holes in inhomogeneous systems: A coordinate-space", Phys. Rev. A, vol. 39, pp. 3761-3767, 1989.

[19] Li, J., et al., "Angew. Chem. Int. Ed., Flexible Hybrid Semiconductors with Low Thermal Conductivity: The Role of Organic Diamines", vol. 48, pp. 7871 –7874, 2009.

[20] Continenza, A., Wentzcovitch, R. M., and Freeman, A. J., "Theoretical investigation of graphitic BeO", Phys. Rev. B, vol. 41, 3540-3544, 1990.

[21] Hohenberg, P., and Kohn, W., "Inhomogeneous Electron Gas", Phys. Rev. B. vol. 136, pp. 864-B871, 1964.

[22] Kohn, W., and Sham, L. J., "Self-Consistent Equations Including Exchange and Correlation Effects", Phys. Rev, vol. 140, A1133–A1138, 1965.

[23] Zerarga, F., Bouhemadou, A., Khenata, R., and Bin-Omran, S., "Structural, electronic and optical properties of spinel oxides $ZnAl_2O_4$, $ZnGa_2O_4$ and $ZnIn_2O_4$", Sol. State. Sci, vol. 13, pp. 1638- 1648, 2011.

[24] Perdew, J. P., Burke, K., and Ernzerhof, M., "Generalized Gradient Approximation Made Simple, Phys. Rev. Lett. 77, pp. 3865- 3868, 1996.

[25] F. Tran and P. Blaha, Accurate Band Gaps of Semiconductors and Insulators with a Semilocal Exchange-Correlation Potential", Phys. Rev. Lett, vol. 102, pp. 226401-226405, 2009.

[26] Blaha, P., et al., WIEN2K: "An Augmented Plane Wave and Local Orbitals Program for Calculating Crystal Properties", edited by K. Schwarz, Vienna University of Technology, Austria 2001.

[27] Tran, F., et al., "Band gap calculations with Becke–Johnson exchange potential", J. Phys. Condens. Matter, vol. 19, pp. 196208- 196216, 2007.

[28] Reshak, A. H., and Khan, S. A.,"Electronic structure and optical properties of $In_2X_2O_7$ (X = Si, Ge, Sn) from direct to indirect gap: An *ab initio* study", Computational Materials Science, vol. 78, pp. 91–97, 2013.

[29] Reshak, A. H., Kamarudin, H., Kityk, I. V., and Auluck, S., "Electronic structure, charge density, and chemical bonding properties of $C_{11}H_8N_2O$ *o*-methoxydicyanovinylbenzene (DIVA) single crystal", journal of material science, vol. 48, pp. 5157-5162, 2013.

[30] Reshak, A. H., Khyzhun, O. Y., Kityk, I. V., Fedorchuk, A. O., Kamarudin, H., Auluck, S., and Parasyuk, O. V., "Electronic Structure of Quaternary Chalcogenide $Ag_2In_2Ge(Si)S_6$ Single Crystals and the Influence of Replacing Ge by Si: Experimental X-Ray Photoelectron Spectroscopy and X-Ray Diffraction Studies and Theoretical Calculations", Sci Adv Mater, vol. 5, pp. 316-327 -12, 2013.

[31] Reshak, A. H., Kityk, I. V., Parasyuk, O. V., Fedorchuk, A. O., Alahmaed, Z. A., Alzayed, N., Kamarudin, H., and Auluck, S., "X-ray photoelectron spectrum, X-ray diffraction data, and electronic structure of chalcogenide quaternary sulfide $Ag_2In_2GeS_6$: experiment and theory", journal of material science, vol. 48, pp. 1342-1350, 2013.

[32] Wooten, F., "Optical Properties of Solids", (New York, Academic Press), 1972.

[33] Penn, D. R., "Wave-Number-Dependent Dielectric Function of Semiconductors", Phys. Rev. B, vol. 128, pp. 2093-2097, 1962.

[34] Fox, M., "Optical Properties of Solids", (New York: Oxford University Press), p. 12, 2001.